MS # *01 Additive Manufacturing of ESAFORM 2025*

Investigations on Material Extrusion Process for Zirconia Filled with a Partially Bio-Based Polymer

AUZENE Delphine[1,a *], ABID Marwa[1,b], BOUDIFA Mohamed[1,c], CHARLON Sébastien[2,d] , ORDINSKI Luc[2,e], LACRAMPE Marie-France[2,f] BARRIERE Thierry[3,g]

[1]CRITT Matériaux Innovation, 9 rue Claude Chrétien, 08000 Charleville-Mézières, France

[2]IMT NE, 941 Charles Bourseul, 59500 Douai, France

[3]Université Marie et Louis Pasteur, Laboratoire de Mécanique Appliquée, 24 rue de l'épitaphe, 25000 Besançon, France

[a]d.auzene@critt-mi.com,[b] marwa.abid@enis.tn, [c] m.boudifa@critt-mi.com, [d] sebastien.charlon@imt-nord-europe.fr, [e] luc.ordynski@imt-nord-europe.fr, [f] marie-france.lacrampe@imt-nord-europe.fr [g]thierry.barriere@univ-fcomte.fr

Keywords: Material extrusion, 3D printing, additive manufacturing, ceramic, zirconia, bio-based binders, debinding, sintering

Abstract

Material Extrusion (MEX) has become an attractive technique for producing filaments for additive manufacturing of complex, low-volume, customized parts. It is an innovative approach to manufacturing ceramic or metal parts by extruding and depositing layer by layer a hot filament made from granules (raw material) or composite filaments. The printed parts are then debinded and sintered to produce the final parts. In this work, a new environmentally friendly raw material was developed from zirconia and partially biobased polymers. Models describing the thermal degradation of polymers were used to calculate the activation energy associated with debinding, and to design the optimal thermal debinding program based on thermogravimetric analysis (TGA). Finally, digital imaging and X-ray tomography were used to characterize the internal morphology of sintered parts.

Introduction

Additive manufacturing of ceramics is an advanced production technology that enables the fabrication of complex and customized components with geometries unattainable through conventional manufacturing methods. Among the various additive manufacturing techniques, Material Extrusion (MEX) offers significant potential for shaping intricate ceramic structures [1,2]. This process involves several key steps, including the preparation of a printable ceramic feedstock, the layer-by-layer deposition of material to form a "green part," and subsequent thermal treatments such as debinding and sintering (Fig. 1) [3].

A critical challenge in this process is the debinding stage, which ensures the complete removal of organic binders without introducing defects in the sample. Inadequate debinding can lead to residual organic compounds that negatively impact the final sintered part, particularly in ceramics [4,5]. Traditionally, debinding is performed using solvent-thermal debinding [6] or thermal

debinding alone [7]. However, optimizing a single thermal debinding cycle without solvent extraction could significantly reduce processing time and cost while maintaining material integrity.

To improve the thermal debinding process, thermogravimetric analysis is commonly employed to quantify the degradation of organic binders by measuring mass loss under controlled heating rates. Additionally, model-free approaches such as Ozawa-Flynn-Wall [8], Friedman [9], and Kissinger [10] provide valuable kinetic parameters, including activation energy, which can be used to design optimized debinding programs [11,12,13,14].

This study aims to investigate the feasibility of a single-step thermal debinding process by testing different binder formulations and optimizing the process parameters. Two distinct feedstocks were developed and processed via the Arburg Plastic Freeforming technique [14], allowing for a comprehensive evaluation of debinding efficiency and its impact on the final material properties.

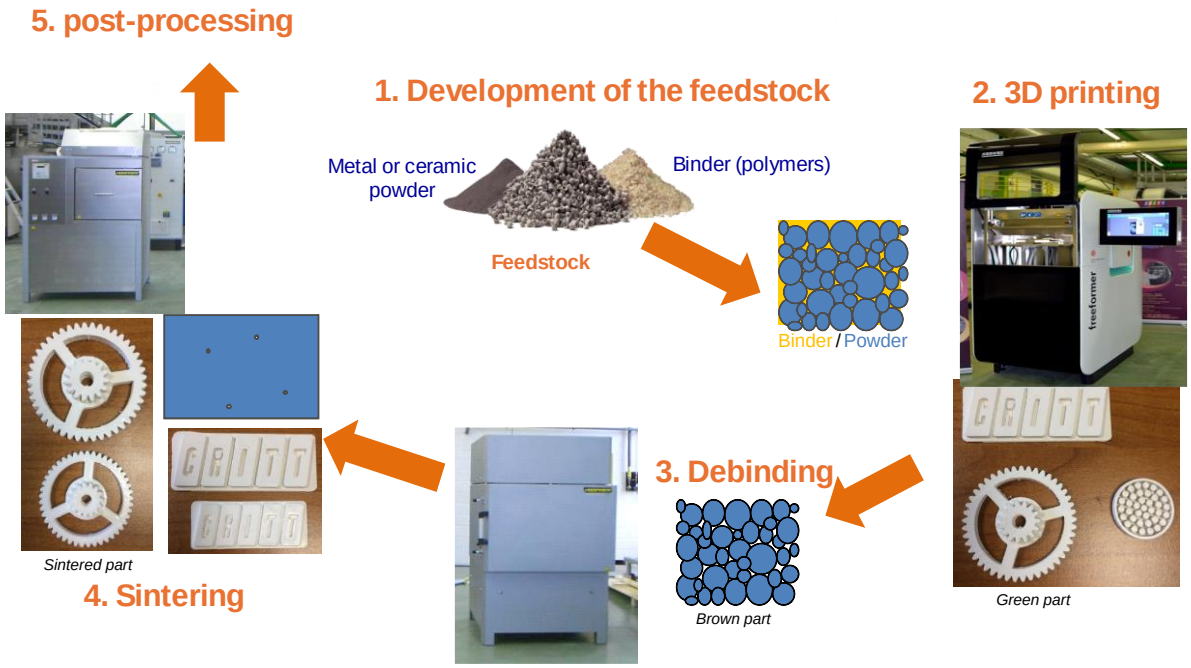

Fig. 1: Additive manufacturing of ceramics based on Material Extrusion process

Methodology

In this work, two feedstocks (A and B) were prepared, containing essentially 3 components:

✓ Powder: Tetragonal zirconia (ZrO_2) TZ-3YS-E, partially stabilized with 3 mol% of yttrium oxide (Y_2O_3), purchased by Tosoh (Japan), supplied as spray-dried granules with an average size D50 = 0.6 µm and a specific surface of 7 ± 2 $m^2.g^{-1}$.

✓ Binders: two binders were considered. feedstock A used a bio-based polyester while feedstock B integrated a polyolefin polymer. Both used also the same amount (in weight) of a water-soluble polymer.

✓ Dispersant: stearic acid, supplied by Sigma-Aldrich, to preserve powder dispersion in the binder and prevent re-agglomeration.

Both feedstocks contained 80 wt.% and 0.4 wt.% of zirconia powder and stearic acid respectively. The zirconia powder was functionalized with stearic acid in ether solvent, then mixed with the binder in a blender for 30 minutes at 20 °C. The mixture was extruded using a twin-screw extruder with 40 rpm rotational speed and a die temperature of T=110 °C and T=180 °C for feedstock A and B respectively.

The feedstocks were printed using a Freeformer machine equipped with a nozzle of 0.25 mm in diameter. The screw and build chamber temperatures were 110 °C and 40 °C for feedstock A and 220 °C and 130 °C for feedstock B respectively. The layer thickness was fixed to 230 µm and 240 µm for feedstock A and B respectively. Discs with a diameter of 20 mm and a thickness of 4mm have been printed, named green parts.

Green parts were thermally debinded in a debinding furnace at different heating rates, then sintered in a sintering furnace. These two steps were carried out under air. To optimize the thermal debinding step, the software NETZSCH Kinetics Neo was used. For this, TGA measurements were carried out on a NETZSCH TG 209 F1 instrument from 25 °C to 450 °C at three heating rates (0.5, 1 and 2 °C/min) under air. Several models have been tested to fit the TGA curves and the Friedman one (Eq. 1) was found to be the most suitable in this work.

$$ln\frac{d\alpha}{dt} = ln\big(Af(\alpha)\big) - \frac{E}{RT} \qquad (1)$$

Where f(α) refers to the reaction mechanism model, A is the pre-exponential factor, E is the activation energy, T the temperature, R is the gas constant and α refers to reaction conversion and is calculated by the Eq. 2:

$$\alpha = \frac{M_0 - M_t}{M_0 - M_f} \qquad (2)$$

where M_0 is the initial mass, M_t is the sample mass at time t; and M_f is the final mass at T=450 °C.

The methodology allows limiting the required time for the debinding step and avoiding a higher mass loss of binding in a low time which must create defects in the part. The optimized debinding steps for both feedstocks are shown Fig. 2.

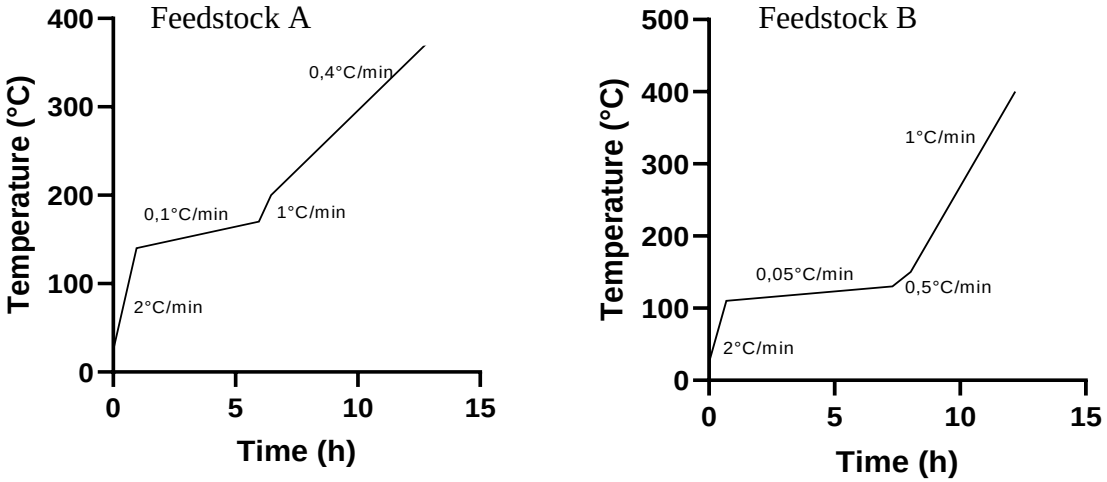

Fig. 2: Thermal debinding step for feedstock A and feedstock B

After the debinding process, the sintering step was carried out under air. The furnace was heated up to 1500°C at a heating rate (50 °C/h) and stayed there for 2 hours. Debinded and sintered parts were characterized by a scanning electron microscope (SEM), after metallization with gold. X-Ray tomography was used to investigate the defects resulting from debinding and sintering steps.

Results and discussion

For polyolefin-based feedstock (B), the optimization of the printing parameters (layer thickness, chamber temperature) allowed to minimize the defects formed during the manufacturing of the green parts. Some defects such as voids and warping remained after printing (not shown here). No defect was observed by X-Ray tomography neither after thermal debinding nor after sintering. SEM observation showed a rough and inhomogeneous morphology after thermal debinding and a well-densified surface after sintering (**Erreur ! Source du renvoi introuvable.**).

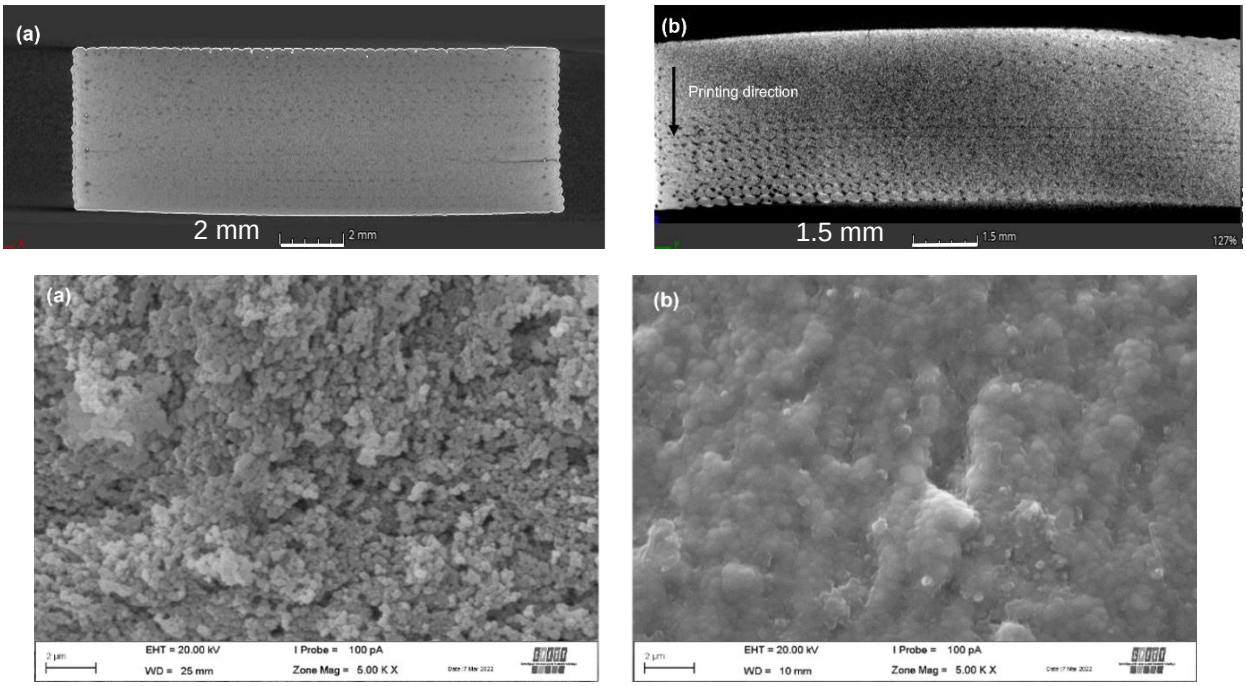

Fig. 3: X-Ray tomography and SEM images of feedstock B after thermal debinding (a) and sintering step (b)

In contrast, X-Ray tomography clearly highlighted the presence of cracks and decohesion between the layers after the thermal debinding of bio-based feedstock (A), these defects being amplified after sintering. SEM analyses revealed dense and homogeneous morphology after debinding and incomplete densification due to the presence of open porosities in the part after sintering (**Erreur ! Source du renvoi introuvable.**).

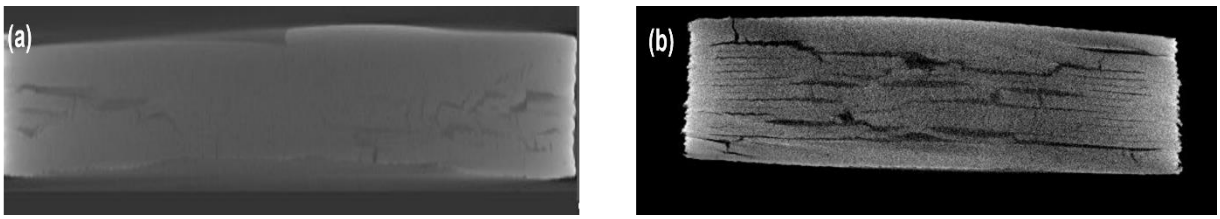

2 mm 2 mm

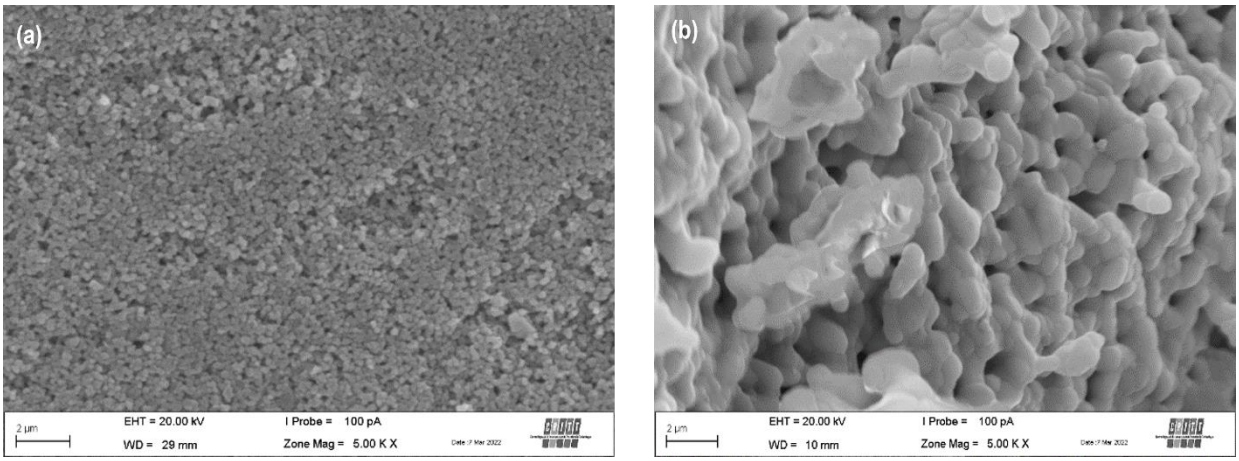

Fig. 4: X-Ray tomography and SEM images of feedstock A after thermal debinding (a) and sintering (b)

The defects formed during the debinding were attributed to an inadequate morphology induced during this step. It was postulated that a strong exothermic reaction (binder degradations) could occur during debinding, leading to a formation of gas inside the parts, which remained entrapped into the part. Stress concentration promoted crack propagation in the specimens (Fig.). These defects were not observed with feedstock B because the presence of open porosities facilitated the gas evacuation formed from the thermal decomposition of binders through the porosities. The absence of porosity in the parts printed for feedstock A seems to hinder the diffusion of gaseous molecules towards the outside of the part.

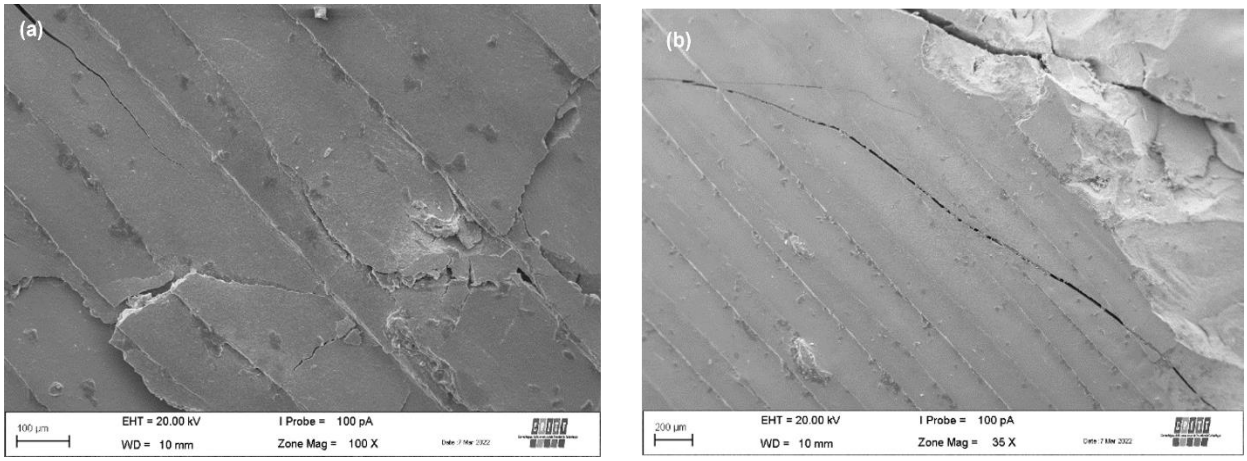

Fig. 5: SEM images showing some defects in the sintered parts (feedstock A)

The binder in feedstocks A and B is made up of different polymers with different degradation kinetics and viscosities during the binder degradation stage. Some studies nevertheless describe the mechanisms involved in thermal debinding. German *et al.* [15] described the binder extraction mechanisms through the powder network, from the core to the outside of the part. Another research group [16] observed, during thermal debinding of a zirconia-based commercial feedstock, a homogeneous distribution of the binder in the part and deduced that the binder is extracted simultaneously from all the pores in the part, whether large or small, whatever their location.

Other works [17] propose a thermal debinding mechanism in three stages and it is this type of mechanism that is observed in the feedstocks that we have developed. Initially, the binder constituents with low molar masses begin to degrade, leaving porosities. In an intermediate phase, the increase in temperature becomes greater and the viscosity of the binder decreases. The pressure of the gases degrading the binder accumulates mainly in the core of the part, more the pore channels are fine and interconnected. This gas pressure then pushes the liquid, low-viscosity binder towards the outside of the part. To encourage this binder to flow outwards, it is important to study the size distribution of the powders and the powder loading rate in the feedstock produced. Finally, in the final phase, most of the binder has been eliminated. Approximately less than 20 % (estimated by mercury porosimetry [17]) of the initial quantity of binder remains. This binder forms pendular bonds that maintain the cohesion of the material.

The work carried out highlights the importance of an initial porosity favouring thermal debinding with the same zirconia powder having the same size distribution and the same filler content for feedstock B. The only difference between the two feedstocks was the polymer mixture component with different degradation profiles (Fig.). The degradation temperatures of the polymer components of feedstock A are very close, complicating the formation of a high-quality sintered part after only one thermal debinding. In contrast, feedstock B presented a significant gap between the degradation temperatures of its polymeric components. In this case, the second polymer remained intact after thermal degradation of the first one and could maintain the shape of the part without formation of too much stress.

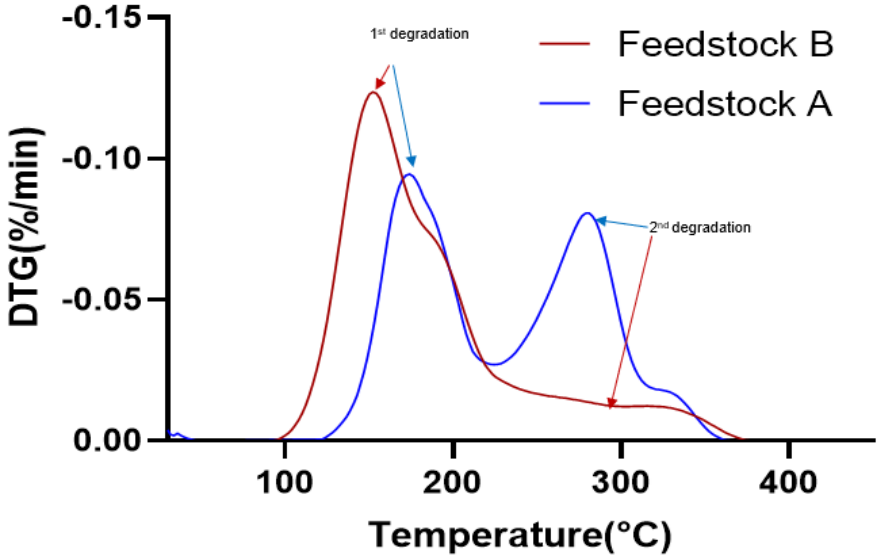

Fig. 6: TGA curves of two feedstocks.

Thus, an alternative to obtain a high-quality part without defects for feedstock A is to perform a binder solvent extraction before the thermal debinding step (*i.e.*: a chemical debinding step). This added step would generate an open-pore structure from the dissolution of the water-polymer component and the second one would then be removed by thermal debinding. Thus, the gas evacuation would be easily done during the thermal debinding step from the existing porosity. The solvent debinding tests were carried out in water at 60 °C for 24 hours.

The following SEM pictures (Fig.) present the morphology of printed specimens for feedstock A after solvent debinding (a) and sintering (b). The solvent debinding was beneficial because it forms interconnected pore structure, that facilitated the thermal debinding step. Also, complete densification was observed after sintering.

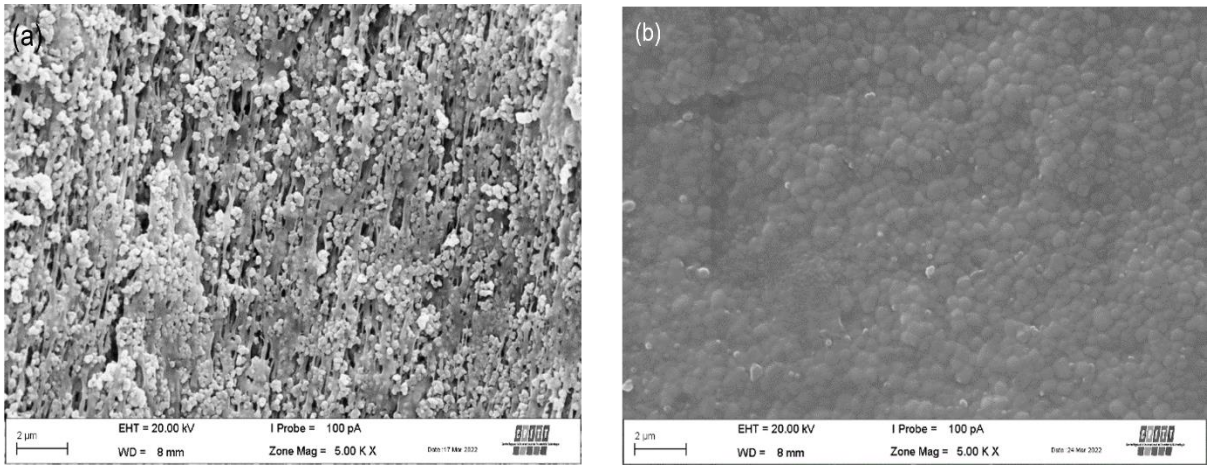

Fig. 7: SEM pictures of feedstock A after solvent debinding (a) and sintering step (b)

Conclusion

Testing a single thermal debinding step for two binders by using the software NETZSCH Kinetics Neo was the major focus of this work. The feedstock containing a polyolefin polymer (Feedstock B) was successfully debinded thermally (*i.e.*: without chemical debinding step) and completely densified after sintering. Only some printing defects were observed which could be overcome by optimizing printing parameters.

The feedstock containing the bio-sourced polymer (Feedstock A) showed some defects after thermal debinding and sintering, caused by an inadequate morphology. To avoid these defects two strategies could be proposed and will be explored in a future step of the present work:

✓ Starting with solvent debinding to facilitate the thermal debinding step by generating several open pores during solvent extraction. It was the easiest solution that was studied in this work.

✓ Optimizing the thermal debinding step by adjusting the heating rate, temperature, and isothermal steps.

Acknowledgments

The authors express their gratitude towards the INTERREG V FWVL, Grand Est region and Wallonia region for the financial support provided for the PEPS project and the contribution of the partners Certech (Be), IMT NE (Fr) and CRITT Matériaux Innovation (Fr). The authors gratefully acknowledge grant CIFRE 2019/1903 from the Agence Nationale de la Recherche et de la Technologie (ANRT, Fr). The authors acknowledge also the contribution of the School of Engineering in Industrial and Digital Sciences (EISINE) at the site of Charleville-Mézières (Fr).

Literature references

[1] G. Herranz, C. Berges, J. Hidalgo, Material Extrusion Additive Technologies: Benefits, Challenges, and Niche Applications, IntechOpen, 2025, https://doi.org/10.5772/intechopen.1008718

[2] J. Gonzalez-Gutierrez, S. Cano, S. Schuschnigg, C. Kukla, J. Sapkota, C. Holzer, Additive Manufacturing of Metallic and Ceramic Components by the Material Extrusion of Highly-Filled Polymers: A Review and Future Perspectives, Materials, vol. 11, no 5, Art. no 5, 2018, https://doi.org/10.3390/ma11050840

[3] C. Rigollet, D. Moinard, Procédés de frittage PIM, in Techniques de l'Ingénieur, vol. M3320, 2011, https://doi.org/10.51257/a-v1-m3320

[4] M. C. Auscher, R. Fulchiron, N. Fougerouse, T. Périé, P. Cassagnau, Zirconia based feedstocks : Influence of particle surface modification on the rheological properties, Ceramics International, vol. 43, no 18, p. 16950-16956, déc. 2017, https://doi.org/10.1016/j.ceramint.2017.09.100

[5] Q. He, Additive manufacturing of dense zirconia ceramics by fused deposition modeling via screw extrusion, Journal of the European Ceramic Society, vol. 41, no 1, p. 1033-1040, janv. 2021, https://doi.org/10.1016/j.jeurceramsoc.2020.09.018

[6] G. Chen, P. Cao, G. Wen, N. Edmonds, Debinding behaviour of a water-soluble PEG/PMMA binder for Ti metal injection moulding, Materials Chemistry and Physics, vol. 139, no 2, p. 557-565, mai 2013, https://doi.org/10.1016/j.matchemphys.2013.01.057

[7] A. Hadian, L Koch, P Koberg, F Sarraf, A Liersch, T Sebastian, F Clemens, Material extrusion based additive manufacturing of large zirconia structures using filaments with ethylene vinyl acetate based binder composition, Additive Manufacturing, Volume 47, November 2021, 102227, https://doi.org/10.1016/j.addma.2021.102227

[8] T. Ozawa, A New Method of Analyzing Thermogravimetric Data, BCSJ, vol. 38, no 11, p. 1881-1886, nov. 1965, https://doi.org/10.1246/bcsj.38.1881.

[9] H. L. Friedman, Kinetics of thermal degradation of char-forming plastics from thermogravimetry. Application to a phenolic plastic, Journal of Polymer Science Part C: Polymer Symposia, vol. 6, no 1, p. 183-195, janv. 1964, https://doi.org/10.1002/polc.5070060121.

[10] H. E. Kissinger, Reaction Kinetics in Differential Thermal Analysis, Analytical Chemistry, Vol 29/Issue 11, nov.1957, https://doi.org 10.1021/ac60131a045

[11] M. Salehi, F. Clemens, T. Graule, B. Grobéty, Kinetic analysis of the polymer burnout in ceramic thermoplastic processing of the YSZ thin electrolyte structures using model free method, Applied Energy, vol. 95, p. 147-155, juill. 2012, https://doi.org/10.1016/j.apenergy.2012.02.025

[12] M. J. G. Fait, E. Moukhina, M. Feist, H.-J. Lunk, Thermal decomposition of ammonium paratungstate tetrahydrate: New insights by a combined thermal and kinetic analysis, Thermochimica Acta, vol. 637, p. 38-50, 2016, https://doi.org10.1016/j.tca.2016.05.009

[13] S. Vyazovkin, ICTAC Kinetics Committee recommendations for analysis of multi-step kinetics, Thermochimica Acta, vol. 689, p. 178597, juill. 2020, https://doi.org/ 10.1016/j.tca.2020.178597

[14] Q. Spiller, J. Fleischer, Additive manufacturing of metal components with the ARBURG plastic freeforming process, CIRP Annals, vol. 67, no 1, p. 225-228, janv. 2018, https://doi.org/10.1016/j.cirp.2018.04.104

[15] R. M. German, Injection molding of metals and ceramics, Powder Metallurgy 42 157-160, vol. 3, 1997, https://doi.org/10.4271/982417

[16] I.M. Somasundram, A Cendrowicz, DI Wilson, ML Johns Phenomenological study and modelling of wick debinding, Chemical Engineering Science, Volume 63, Issue 14, July 2008, Pages 3802-3809, https://doi.org/10.1016/j.ces.2008.04.040

[17] K. S. Hwang, T. H. Tsou, Thermal debinding of powder injection molded parts: Observations and mechanisms, Metall Trans A, vol. 23, no 10, p. 2775-2782, oct. 1992, https://doi.org/10.1007/BF02651756